Electrical Model and Electrical Temperature-Dependent Model for Electrospray Thrusters

Francisco José Blázquez-Plaza, Andrés Barrado, *Senior Member, IEEE*, Mick Wijnen, and David Villegas-Prados

***Abstract*—This article presents two equivalent electrical models of electrospray thrusters verified with experimental data. The first model presented in this article aims to improve the electrospray thruster representation in HV-dc/dc converter's steady-state and closed feedback-loop response simulations since it is one of the most critical subsystems of an electrospray propulsion system. The proposed model, adapted from cold cathode fluorescents lamps (CCFLs) models, is composed of basic electrical elements (resistors, capacitors, and diodes), and it is implemented in SIMULINK/MATLAB. The model parameters are extracted from experimental data, and it is possible to export them to any electrical simulation tool. The second model incorporates temperature dependencies based on electrospray physics to predict the thruster's behavior within an experimental data set. The absolute error between the experimental and simulated data is less than two microamps for the nontemperature-dependent model and two and five-tenths microamps for the temperature-dependent model in the thruster's operating range. Besides, the relative error is less than 4% for the nontemperature-dependent model and less than 8% in the thruster's operating range for the temperature-dependent model. A comparison with previous models is quantified showing that the models presented in this article are a better approximation, validating the proposed models.**

***Index Terms*—Electrospray thruster, equivalent model, experimental verification, *I–V* curve, nonlinear load, simulation, temperature-dependent model.**

I. Introduction

In THE past few decades, the quick development of electric propulsion systems has promoted big changes in related industry fields. Electrospray thrusters are presented as a very attractive alternative to traditional electrical propulsion systems. Due to low efficiencies, large volumes, and thermal management issues, existing propulsion technologies make adoption difficult. Electrospray propulsion systems, with their extremely high efficiency at low power and compact form factor [1], could unlock the mass incorporation of propulsion systems in small satellites [2] (stimulated by technology miniaturization), microsatellites, or nanosatellites platforms, enabling on-orbit mobility for the spacecraft [3], [4].

Electrospray thrusters are commonly designed and tested independently from flight electronics to reduce the possibility of failure during the thruster development phase since achieving a stable and repeatable thruster emission needs a long iterative process still under research. This increases the design uncertainty of the power stage. One of the key parts of the electronics design is to develop highly accurate device models that guarantee the accuracy required for both steady and transient states without excessively increasing the model complexity [5].

In addition, the physical and analytical approaches, based on exploiting the physical and geometric properties of the electrospray thruster, together with the fact that the propulsion system implies the combination of several subsystems [6], [7] together (e.g. thruster, dc/dc converter, sensor, control unit...), are difficult to select and optimize system's operating parameters by adopting conventional modeling and software simulation tools.

The experimental *I–V* curves can be computed and used to guide the development during the development of the HV-dc/dc converters (specifically in topologies where the converter gain is dependent on both output current and voltage), making it an attractive choice for modeling and simulation instead of assuming an equivalent load resistor. A precise control design is mandatory to supply electrospray thrusters since the load profile can vary dramatically during operation due to multiple factors (e.g. temperature, thruster contamination, and aging). The control stage shall include a wide stability margin and soft-start techniques to avoid failures. In addition, a precise representation at the operation point is needed to calculate the converter's efficiency.

This paper article presents a novel model of the electrical behavior of an electrospray thruster. The model is verified with experimental data using basic elements on MATLAB/Simulink software with the possibility to export component parameters to any electrical simulator. The model presented allows for designing based on experimental data. In addition, the derivation of the model to a novel temperature-dependent model is included. By incorporating temperature as a variable, the model offers enhanced predictive capabilities and opens new avenues for

Manuscript received 24 April 2023; revised 12 June 2023; accepted 1 July 2023. Date of publication 5 July 2023; date of current version 1 September 2023. This work was supported by the Comunidad de Madrid through the research project IND2022/TIC-23688. Recommended for publication by Associate Editor M. Ponce-Silva. *(Corresponding author: Francisco José Blázquez-Plaza.)*

Francisco José Blázquez-Plaza is with the Electrical Engineering, Universidad Carlos III de Madrid - Campus de Leganes, 28911 Leganes, Spain (e-mail: francisco.blazquez@ienai.space).

Andrés Barrado is with the Tecnologia Electronica, Universidad Carlos III De Madrid, 28911 Leganes, Spain (e-mail: andres.barrado@uc3m.es).

Mick Wijnen is with IENAI Space S.L., 28911 Leganes, Spain (e-mail: mick.wijnen@ienai.space).

David Villegas-Prados is with the Universidad Carlos III de Madrid - Campus de Leganes, 28911 Leganes, Spain (e-mail: david.villegas@ienai.space).

Color versions of one or more figures in this article are available at https://doi.org/10.1109/TPEL.2023.3292421.

Digital Object Identifier 10.1109/TPEL.2023.3292421

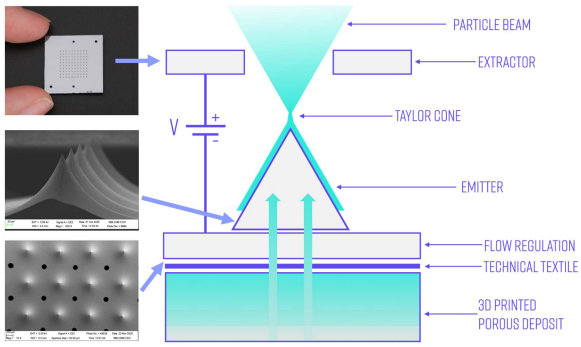

Fig. 1. Electrospray thruster working principle.

design optimization since thermal effects can be critical for an accurate operation.

The rest of this article is organized as follows. Section II provides a comprehensive overview of electrospray physics. In Section III, existing models in the literature are reviewed and a novel improved model is presented. The model verification process with MATLAB/Simulink using experimental data from the ATHENA-XM0 electrospray thruster, together with an error analysis, is presented in Section IV. Section V examines the impact of temperature variability on the behavior of electrospray thrusters and presents a novel temperature-dependent model based on how parameters vary with temperature in the electrospray thrusters. In Section VI, the models presented in this article are compared with previously published models using experimental data from the ATHENA-XM0 electrospray thruster to validate their accuracy. Finally, Section VII concludes this article with key findings and implications.

II. Introduction to Electrospray Physics

Electrospray thrusters are based on the electrostatic extraction and acceleration of particles from conductive liquids, predominantly ionic liquids (IL). IL are room-temperature molten salts composed of chemically stable mixtures of positive and negative molecular ions [4]. Fig. 1 describes the physical working principle. To be able to achieve the high electric fields needed for electrospray emission, electrospray thrusters contain sharp needle-like features that concentrate the electric field at their tip. Since these needles are generally of the order of hundreds of micrometers, and the individual emission and corresponding thrust are very limited, these needles are multiplexed into arrays (generally on a single square chip) called an emitter. An emitter is combined with an extractor, which is another chip of similar size with an array of apertures that are aligned with the needles (or cones) of the emitter. The IL is fed to the emitter from below and migrates to the tip of the needles by capillary forces. The surface of the liquid is then deformed due to the electric field and the balance of electrostatic and hydrostatic forces results in the formation of a Taylor cone [8]; however, depending on the conditions, this can also be a dome [9].

Electrospray thrusters can emit in both polarities. This allows to reduce effects of spacecraft charging without an additional neutralizer or cathode as needed in plasma-based propulsion systems [10], and therefore in their power converters [11], [12].

The current versus voltage (*I–V*) curve describes the electrical response of an electrospray thruster. This curve is nonlinear; besides, the positive and negative emissions are asymmetrical.

The voltage value at which a capillary thruster starts emitting current is referred to as startup voltage [13], given by V_0 (1) and depends on three factors: liquid's surface tension (γ), emitter–extractor distance (2), and cone radius (r). Below this voltage, the surface tension forces counteract the electrostatic force not allowing emission. ε_0 corresponds to vacuum permittivity.

$$V_0 \approx \sqrt{\frac{\gamma r}{\varepsilon_0}} ln\left(\frac{2D}{r}\right). \tag{1}$$

The emitter current is controlled by the applied voltage and, therefore, thrust (since the electric field accelerates ions to a high-speed jet [14]). The velocity, u, of emitted ions, i particle, (and specific impulse) vary with the square root of the applied voltage, V, as shown in (2), where ξ_i is the specific charge of the particle.

$$u_i = \sqrt{2\xi_i V}. \tag{2}$$

Equation (3), presented by Coffman [9] ($\hat{X}$ as the normalized value and X^* as the reference value), is the expression for the normalized current ($\hat{I} = I/I^*$) as a function of the normalized electric field ($\hat{E} = E_n^v/E^*$) at pure ion emission regime for a capillary emitter, where only ions are emitted as opposed to only droplets or a mixture of ions and droplets.

$$\hat{I} = \frac{1}{\hat{E}^3\left[1 + \chi e^{\psi\left(1-\sqrt{\hat{E}}\right)}\right]}. \tag{3}$$

The dimensionless quantity, χ, is equal to the ratio of the characteristic charge relaxation time and the characteristic emission time, and ψ is another dimensionless quantity generally of the order of 40–80 [9]. The normalized electric field is directly proportional to the applied voltage, scaled by some constant depending on the emitter/extractor geometry.

This relationship captures empirical trends in at least a qualitative way [9]. Nevertheless, in experimental work, it is found that the *I–V* characteristics can be described by an approximation to a simple exponential fit of the form of (4) [15], where I_0 and N are fit constants. This approximation ease the analysis of experimental data but is not a design model that can predict the *I–V* characteristics [15].

$$I = I_0(T)e^{\left(\frac{V}{V_0(T)}\right)^N}. \tag{4}$$

Equation (4) is similar to Shockley equation [16] for an ideal diode and becomes the starting point of the model proposed in this article.

III. Electrospray Thruster Equivalent Model

A. Previous Approaches.

Electrical *I–V* response can be modeled with a current-dependent behavioral current source as presented in (4) [15] and as in (5) by Hicks [17].

The piecewise function is described in (5) for positive emission (the negative emission is obtained by simply inverting the emitted current sign).

$$I(V) = \begin{cases} AV\left(e^{B\sqrt{V}}\right), & V \leq V_0 \\ \frac{(V-V_0)^2}{m}, & V > V_0. \end{cases} \tag{5}$$

At voltages lower than the start-up voltage (V_0), the emission behavior is approximated with an exponential relationship. On the other hand, a quadratic approximation is used at voltages higher than the start-up voltage. The approximations meet at the start-up voltage and provide a smooth transition. The exponential model is controlled by two parameters, A and B, which relate to the activation energy of the process and other physical constants, being a similar approximation compared with (4). The emission behavior after the exponential field emission regime can be approximated as a linear fit for each emission site. Two parameters control the quadratic emission profile, the startup voltage, V_0, and a constant factor to control the steepness, m.

However, HV-dc/dc converters for electrospray thrusters papers, as [18], [19], [20], and [21], do not include an electrical model for the load. The design is at the operation point with a linear resistance (R) approximation. This approximation results in (6), assuming that there is no emission before the start-up voltage. It does not take into account either the nonlinear behavior of the device or the complex physical processes underlying the state change. An accurate load modeling becomes mandatory to properly operate the electrospray thruster, making the approximation of (6) insufficient.

$$I(V) = \begin{cases} 0, & V \leq V_0 \\ \frac{V-V_0}{R}, & V > V_0. \end{cases} \tag{6}$$

Digital control can overcome the limitations when combined with a more accurate model, implementation of sophisticated control laws, taking care of nonlinearities, parameter variations, or construction tolerances using self-analysis and autotuning strategies. Besides, it is also possible to modify the control strategy, or even to reprogram it, without the need for significant hardware modifications. The use of a digital control strategy will present higher tolerance to signal noise and will be able to overcome the aging effects or thermal drifts [22].

A better approximation is found in [23], where is modeled as an electrical circuit with a voltage source in series with a diode and a resistor, resulting in the following:

$$V = IR + \frac{1}{C_2}\ln(1 + I/C_1). \tag{7}$$

The constants $C1$ and $C2$ depend on the parameters of the experimental setup and replace the saturation current and emission coefficient of a diode. This constants vary with emitter geometry and emitter-to-extractor separation distance, temperature, and liquid's properties [23].

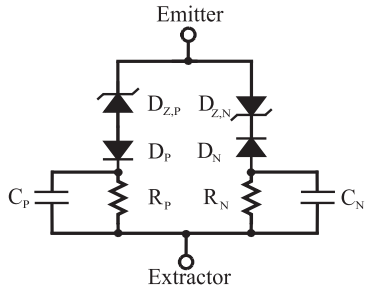

Fig. 2. Proposed electrical equivalent circuit for the electrospray thruster.

B. Proposed Model.

Fig. 2 represents the model chosen to describe the *I–V* response of the electrospray thruster. The presented model is based on the equivalent cold cathode fluorescent lamp (CCFL) electrical model circuit [24]. The model presented in this article is a novel contribution to the field of power electronics in electrospray applications improving previous approaches by updating the CCFL model for electrospray applications. Since the electrospray thruster is not symmetrical, each polarity is modeled by independent but equal components. Component polarity actuation is clarified with a subindex as the way as X_P for positive and X_N for negative (the model presented in [24] for CCFL only includes one polarity).

The circuit's scheme is constituted (per polarity) by the following.

1) *Zener diode D_Z:* This represents the zero current region when $V < V_0$.
   The Zener diode is governed by (8) [16]. V_0 is the diode's breakdown voltage, in the model the start-up voltage. R_Z is a low parasitic resistance assumed to be less 1 mΩ and, therefore, negligible.

$$V_{D,Z} = V_0 + IR_Z \approx V_0. \tag{8}$$

2) *Diode D:* This represents the exponential region.
   The diode is governed by Schokley (9) [16]. I_S is the diode's saturation current, which varies with temperature in a regular diode. n is the emission coefficient, and its value depends on the material and structure of the diode.

$$I_D = I_S\left(e^{\frac{V_D}{nV_T}} - 1\right). \tag{9}$$

   V_T (10) is the thermal voltage; here, k is Boltzmann's constant, T is the absolute temperature of the p-n junction, and q is the magnitude of charge of an electron. The diode's reverse breakdown voltage is assumed to be infinite.

$$V_T = \frac{kT}{q}. \tag{10}$$

3) *Resistor R:* This represents the linear region.

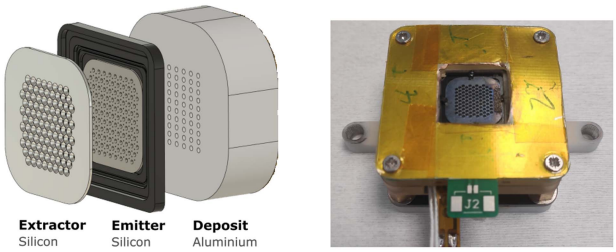

Fig. 3. ATHENA-XM0 thruster head. (a) Exploded view. (b) Experimental assembly.

Electrospray thrusters emit current in the range of 10–1000 μA. Therefore, on the model, R is assumed to be a large resistance of at least 100 kΩ.

4) *Capacitor C:* This represents the parasitic capacitance generated by the thruster assembly.
Capacitance is calculated by biased parallel plate (11), where ε_0 is vacuum permittivity, d distance between plates, and A is plate's area.

$$C = \frac{\varepsilon_0 A}{d}. \tag{11}$$

Measurements have shown that the capacitance is on the order of tens of picofarads (experimental measurement shows a value of 30 pF for the ATHENA-XM0 thruster when determining the value that yields the closest-to-zero emitted current (I) from the emitter voltage (V) in $I - C\frac{dV}{dt} = 0$, while introducing a signal around 100 V lower than V_0. However, its influence is not critical since it will act as an open circuit once it is charged.

Applying Kirchhoff's second law to the series combination of D_Z, D, and R results in (12). This equation describes the *I–V* response of the electrospray thruster model for positive emission (the negative emission is obtained by simply inverting the emitted current sign).

$$V = V_0 + RI + nV_T \ln(1 + I/I_S). \tag{12}$$

The equation shall be solved for the positive and the negative components with an iterative approximation method to obtain the parameter values of the components since it is not possible to solve them directly. As the model is just composed of basic elements, it is possible to export it to any electrical simulation tool.

IV. Experimental Verification of Presented Model Using MATLAB/Simulink

A. Experimental Setup

Experimental curves have been used to verify the proposed model. The waveforms belong to IENAI Space ATHENA-XM0 electrospray thruster [see Fig. 3(b)], composed by an externally wetted emitter array of 101 micro cones with a nanotexturization, which also has been published in [25]. The thruster has been excited with triangular waveforms from −1300 to 1300 V at temperatures of 30°C, 40°C, and 50°C [being this the thruster's

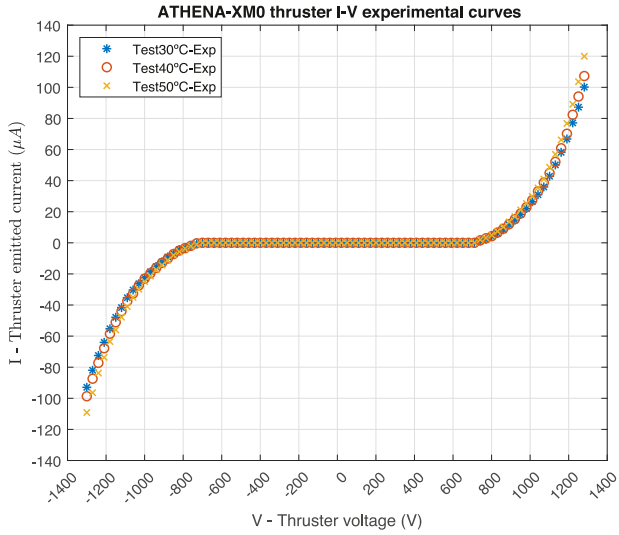

Fig. 4. ATHENA-XM0 *I–V* experimental curves.

temperature range for the experimental setup of Fig. 3(b) due to assembly materials constraints]. Every test has been conducted at a consistent propellant temperature, which is regulated by a heater with a control loop with an error tolerance of 0.1°C. Emission tests have confirmed that this electrospray thruster exhibits stable emitted current within the specified voltage and temperature range. The thruster is designed to operate in the pure ionic regime, which means that voltages below 1000 V should not be applied during regular operation. Hence, the ATHENA-XM0 has an operational voltage range of 1000 to 1400 V and −1000 to −1400 V for positive and negative polarities, respectively. Applying voltages above 1400 V could damage the emitter due to emitter–extractor distance constraints. Moreover, the propellant temperature affects the thruster's operational response [25]. The IL used in this work is 1-ethyl-3-methyl-imidazolium bis(trifluoromethylsulfonyl)imide, also known as EMIM-Im in the literature. The experimental *I–V* curves, depicted in Fig. 4, reveal that the emitted current varies depending on the temperature.

B. Parameter Extraction

Simulation component parameters are extracted by fitting a nonlinear-least-squares approximation method to the curves presented in Fig. 4. Using the least absolute residuals (LAR) method shows a better goodness-of-fit, minimizing the absolute difference of the residuals rather than the squared differences of the bisquare method. Consequently, extreme values, such as undesirable spikes, have a lesser influence on the fit. In addition, the trust-region algorithm has been selected.

Tables I–III include extracted values for each experimental data set (Test30°C, Test40°C, and Test50°C, respectively) where the approximation method has been computed for both polarities.

The increase in temperature leads to a clear increase in the emitted current, as the conductivity of the liquid rises [25]. The asymmetry in the emitted current arises due to the distinct

TABLE I
TEST30°C—EXTRACTED COMPONENT VALUES

Test30°C			
Component	Equation (12) Parameter	Value	Units
$D_{Z,P}$	V_0	727	V
D_P	n	9423	-
	I_S	12	μA
R_P	R	101	kΩ
$D_{Z,N}$	V_0	730	V
D_N	n	8775	-
	I_S	11	μA
R_N	R	512	kΩ

TABLE II
TEST40°C—EXTRACTED COMPONENT VALUES

Test40°C			
Component	Equation (12) Parameter	Value	Units
$D_{Z,P}$	V_0	720	V
D_P	n	8583	-
	I_S	11	μA
R_P	R	120	kΩ
$D_{Z,N}$	V_0	725	V
D_N	n	8925	-
	I_S	11	μA
R_N	R	252	kΩ

TABLE III
TEST50°C—EXTRACTED COMPONENT VALUES

Test50°C			
Component	Equation (12) Parameter	Value	Units
$D_{Z,P}$	V_0	713	V
D_P	n	8126	-
	I_S	11	μA
R_P	R	100	kΩ
$D_{Z,N}$	V_0	720	V
D_N	n	8901	-
	I_S	12	μA
R_N	R	100	kΩ

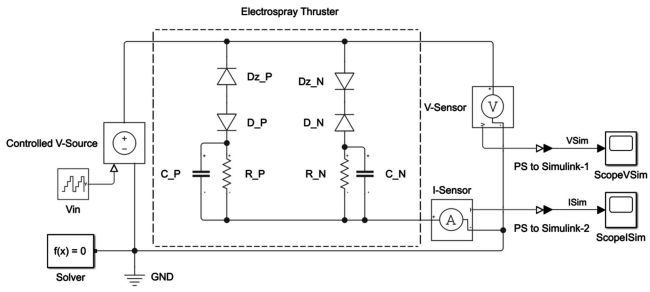

Fig. 5. Electrospray thruster electrical equivalent circuit—Simulink Sch.

mobility of negative and positive particles, resulting from their disparate masses [25]. The evolution of all parameters as a function of temperature follows the expected trend, except for R_P, which does not exhibit the same behavior. In addition, due to the disparate of masses, R_N is strongly affected by temperature compared with R_P.

C. Simulation and Error Analysis

Fig. 5 illustrates the circuit for simulation constituted by the following.

1) Electrospray thruster model with SIMSCAPE elements based on Fig. 2.
2) *Vin:* experimental voltage data array input as a counter from the minimum to the maximum voltage.
3) Voltage-controlled source that replicates Vin array.
4) Voltage and current sensors.

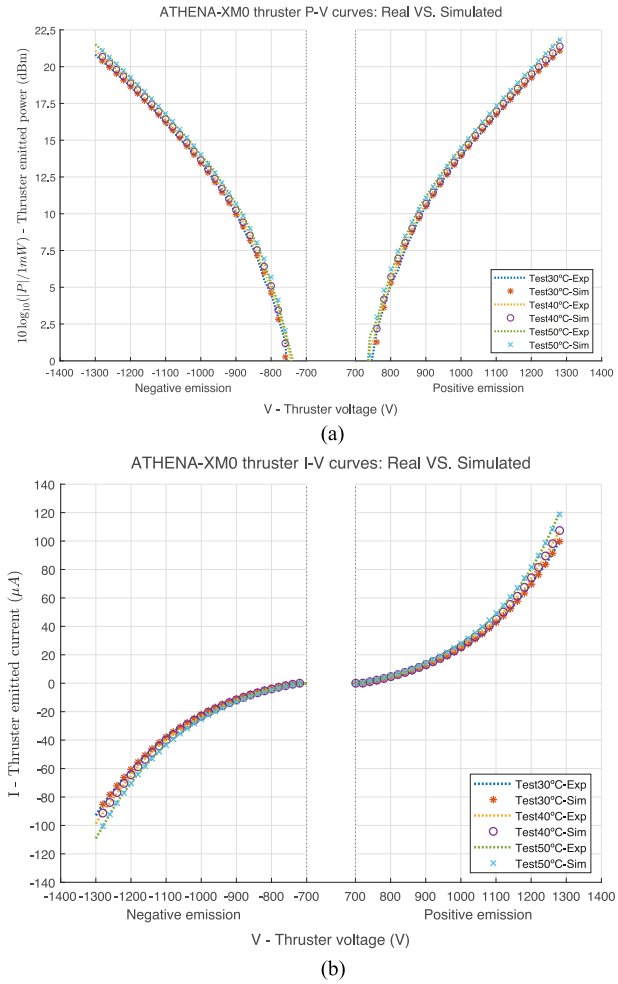

Fig. 6. Athena-XM0 curves (emission area): real versus simulated. (a) *P–V* (dBm-V). (b) *I–V* (μA-V).

5) Scopes to export simulation data to workspace through physical-to-Simulink signal converter block.

The deviation between simulated and experimental curves in terms of emitted power is shown in Fig. 6(a). It can be assumed that the thruster is operating above 1 mW; therefore, the curves have been expressed in decibels per milliwatt (dBm) to ease the comparison of the curves (0 dBm = 1 mW), and to identify trends. On the other hand, a detailed view of the compared *I–V* curves is shown in Fig. 6(b) for positive-emission and negative-emission areas, respectively. It can be clearly seen that simulated curves are close to real ones in the full range of experimental input data. Nonemission area has been omitted since its value is zero for both real and simulated curves.

In addition, the absolute and relative current error graphs between simulated and experimental curves are shown in Fig. 7.

To operate the electrospray thruster, a soft start is needed in the power converter to prevent excessive inrush current from flowing into the thruster and to avoid damage to the emitter. A sudden increase in current can cause electromechanical stress on the emitter, which can disrupt the ionization process and affect thruster performance. A soft-start ensures a gradual increase in the voltage to the thruster, reducing the risk of damage to

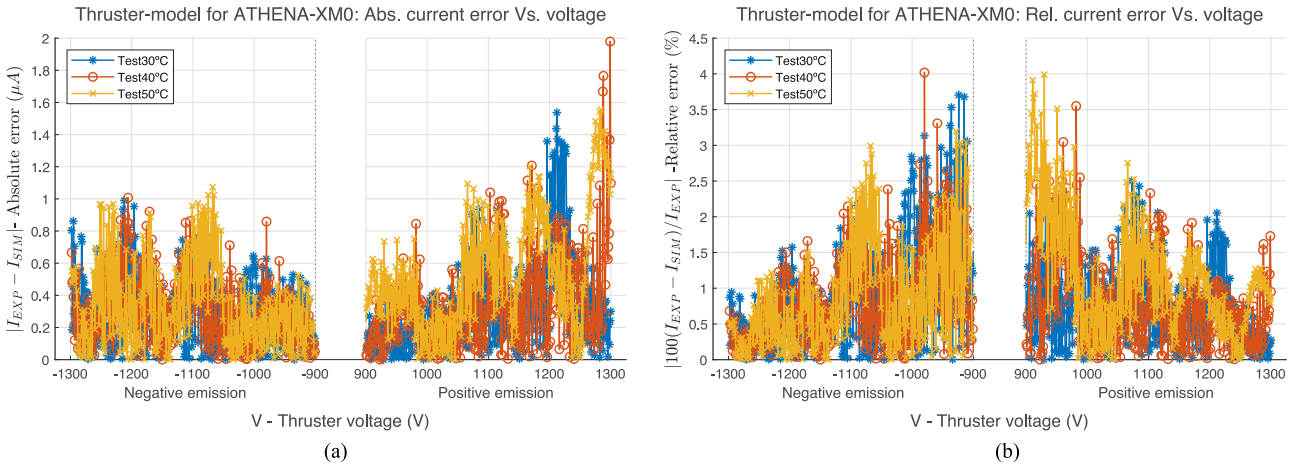

Fig. 7. Computed current error curves for Athena-XM0 experimental curves. (a) Absolute error. (b) Relative error.

the emitter electrodes and improving the overall stability and performance of the thruster system. ATHENA-XM0 should operate in the voltage range of 1000 to 1400 V and -1000 to -1400 V for positive and negative polarities, respectively, for device stability. The accuracy of the current sensor is $\approx 1\,\mu$A.

Therefore, the range of error in Fig. 7 is $|900 - 1400|$V considering $|900|V$ as the initial voltage value in regular operation, which will be increased to the nominal operating point.

For the experimental data presented in this article, the model presents less than 4% error in the full range shown in Fig. 7(b). In addition, the model absolute error is always below 2 μA, which is a very low quantity of error considering a sensing accuracy of $1\,\mu$.

The adequacy and accuracy of the model structure and LAR fitting procedure have been demonstrated to represent the *I–V* curve effectively. To introduce the model parameters within the working range, a lookup table is assumed to be utilized in the simulation. A comparison with the models presented in the literature is included in Section VI.

V. Behavior Predictions: Temperature-Dependent Model

Thruster behavior variations occur during the system's lifetime due to electrochemical degradation. Furthermore, extractor contamination can produce arcs, which generate an overcurrent state and modify the steady-state operation. In addition, aspects such as aging, spacecraft charging, emitter degradation due to the IL properties, and temperature (as presented in this paper) affect the *I–V* curve of the electrospray thruster. Therefore, the design of the control stage shall consider the nonlinear and time-variable thruster performance, not only at the operation point but including the start-up and full dynamic range.

It is not possible to fully characterize a thruster over thousands of operating conditions; therefore, the capability to predict operating points from simulations based on limited experimental data becomes increasingly important. This section shows how the model is adapted to predict the thruster operation variations based on experimental curves at different temperatures originating a temperature-dependent model.

TABLE IV
Properties of Athena-XM0 With 1-Ethyl-3-Methyl-Imidazolium Bis(Trifluoromethylsulfonyl)Imide At Different Temperatures

Temperature $T(^\circ C)$	**Start-up voltage:** $V_{0,P} - V_{0,N}(V)$ $(Experimental)$	**Viscosity** $\mu(mPa \cdot s^{-1})$ ([26] [27] [28])	**Surface tension** $\gamma(mN \cdot m^{-1})$ ([26] [27] [28])
20	-	36.50	33.79
30	727 - 730	25.70	32.86
40	720 - 725	19.05	31.99
50	713 - 720	14.65	31.16
60	-	11.39	30.34

Equation (12) includes operating temperature with V_T term where the temperature of the equivalent diode can be included but the approximation of n corrects any divergence to the best approximation possible. Therefore (12) has been adapted to include the operating temperature of the electrospray thruster. The electrospray thruster parameters that are temperature dependent and affect the *I–V* curve are [25]: viscosity (μ), surface tension (γ), and start-up voltage (V_0). The different values of each parameter for previous experimental curves have been included in Table IV. Start-up voltage has been defined as the point where the emitted current is above 1 μA and has been extracted experimentally. On the other hand, the parameters that depend on liquid properties have been obtained from [26], [27], and [28] in the 20 °C–60 °C range.

Equation (1) [29] approximates the start-up voltage for an electrospray thruster. This equation is governed by constants determined by the thruster geometry (explained in detail in [29], where D is the distance between the emitter to the extractor and r is the cone radius) except for the surface tension (γ). Hence, $V_0(T)$ can be approximated by $\sqrt{C_1 + C_2\,T}$ into the electrical model (in the Zener component), as shown in Fig. 8, based on the experimental data included on Table IV.

A regular resistor vary with temperature as $R = R_0(1 + \Delta T)$[16]. However, the resistance of an electrospray emitter depends on the liquid's viscosity. Slotte (13) [30] is used in

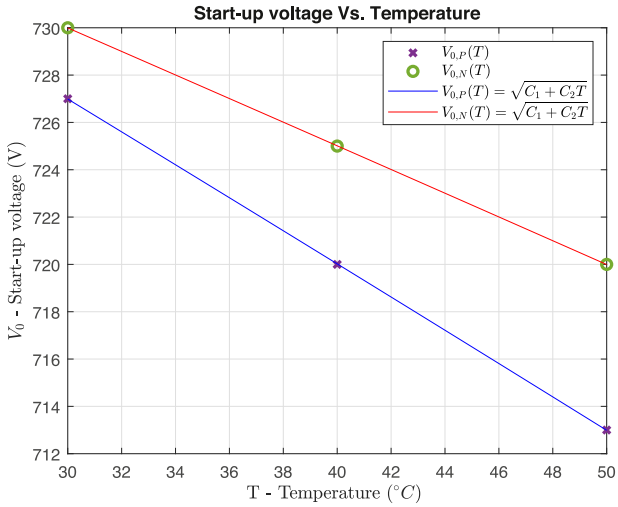

Fig. 8. Experimental setup start-up voltage versus temperature approximations, $V_0(T)$.

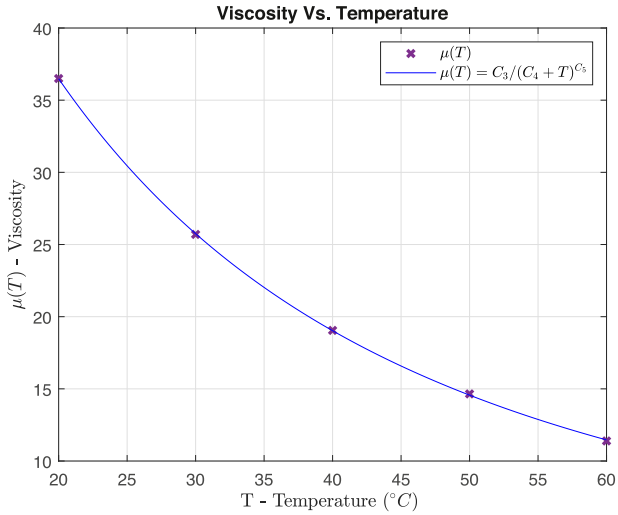

Fig. 9. Experimental setup viscosity versus temperature approximation.

numerical approximations for relating the viscosity with temperature.

$$\mu \approx \frac{C_3}{(C_4 + T)^{C_5}}. \tag{13}$$

The resistance can be approximated by fitting the behavior of the viscosity with Slotte equation, as shown in Fig. 9.

The emission coefficient of a diode, n, multiplied by the voltage produced within the p-n junction due to the action of temperature, V_T, can be approximated by $C_6\,T$. As well as assumed in [16], since the saturation current varies proportionally with the temperature for a regular diode, the assumption that it varies in the electrospray thruster electrical model has been adopted as $I_S(T) = \frac{1}{C_7 + C_8\,T}$.

Given these points, the expression of the *I–V* response with temperature dependency of the electrospray thruster for the electrical model is presented in (14), where $C_1 - C_8$ are the

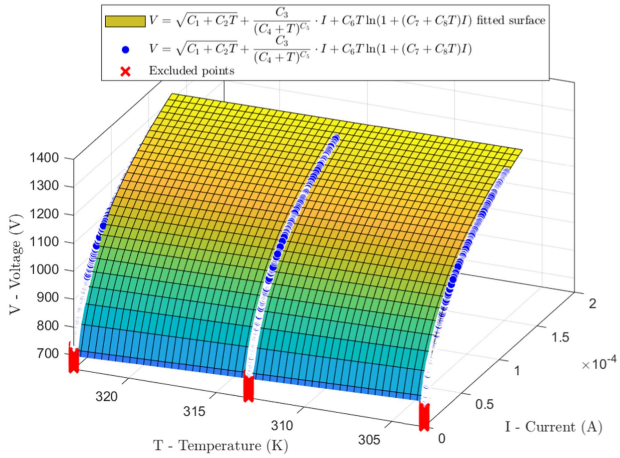

Fig. 10. Temperature-dependent surface extracted for ATHENA-XM0 from 30 °C to 50 °C, 303.15 to 323.15 K, for positive polarity.

fitting constants.

$$V = \sqrt{C_1 + C_2\,T} + \frac{C_3}{(C_4 + T)^{C_5}} \cdot I + C_6 T \ln\left(1 + (C_7 + C_8\,T) I\right) \tag{14}$$

where the electrical model is represented as follows:

1) Zener $V_0 = \sqrt{C_1 + C_2\,T}\ (V)$;
2) $R = C_3/(C_4 + T)^{C_5}\ (\Omega)$;
3) $n = C_6\,T/V_T$;
4) $I_S = 1/(C_7 + C_8\,T)\ (A)$.

A. *Parameter Extraction for Temperature-Dependent Model*

Such as in the previous section, the simulation component parameters are extracted by fitting a nonlinear-least-squares approximation method. Contrary to the previous case, the fitting includes all experimental curves to create a surface that allows making predictions based on operating temperature. This surface is shown in Fig. 10 for positive polarity (negative polarity is achieved by computing the algorithm again inverting the sign).

Table V includes extracted constants for the generated surface, where the approximation method has been computed for both polarities.

B. *Simulation and Error Analysis for Temperature-Dependent Model*

The model has been verified with the same procedure as the nontemperature-dependent model using the simulation circuit of Fig. 5.

Fig. 11 compares the *I–V* characteristics of the electrospray thruster. It can be observed that simulated curves are close to real ones in the full range of experimental input data. No emission area has been omitted in the figure since it is zero in both simulated and experimental curves.

In addition, the absolute and relative emitted current error graphs between simulated and experimental curves are shown in Fig. 12.

TABLE V
TEMPERATURE DEPENDENT MODEL EXTRACTED CONSTANTS FOR ATHENA-XM0 FROM 30 °C TO 50 °C

	C_1	C_2	C_3	C_4	C_5	C_6	C_7	C_8
Positive	$-3.18 \cdot 10^3$	$1.52 \cdot 10^6$	$5.94 \cdot 10^{-1}$	$8.31 \cdot 10^{-1}$	$3.74 \cdot 10^1$	$7.85 \cdot 10^{-1}$	$2.38 \cdot 10^{-14}$	$8.07 \cdot 10^4$
Negative	$-3.19 \cdot 10^3$	$1.53 \cdot 10^6$	$6.19 \cdot 10^1$	$1.70 \cdot 10^1$	$7.76 \cdot 10^0$	$8.44 \cdot 10^{-1}$	$2.38 \cdot 10^{-14}$	$7.69 \cdot 10^4$

TABLE VI
COMPARISON OF PRESENTED MODELS VERSUS MODELS FROM LITERATURE WITH EXPERIMENTAL DATA TEST40°C

	Assigned ID	Components (per polarity)	Equation	Reference	Max. Absolute Error (μA)	Max. Relative Error (Positive, %)	Max. Relative Error (Negative, %)
Equation Model from this study Zener+Diode+(Resistor||Capacitor)	A	4	(12)	-	1.98	2.33	2.39
Equation Model (T) from this study Zener+Diode+(Resistor||Capacitor)	B	4	(14)	-	1.82	2.25	2.55
Resistor above start-up voltage	C	2	(6)	[18] [19] [20] [21]	19.33	42.25	37.69
Resistor+Diode	D	2	(7)	[23]	7.56	19.04	14.68
Exponential function (Behavioral current source)	E	1	(4)	[15]	9.23	6.33	9.36
Piece-wise function (Behavioral current source)	F	1	(5)	[17]	2.49	3.85	4.09

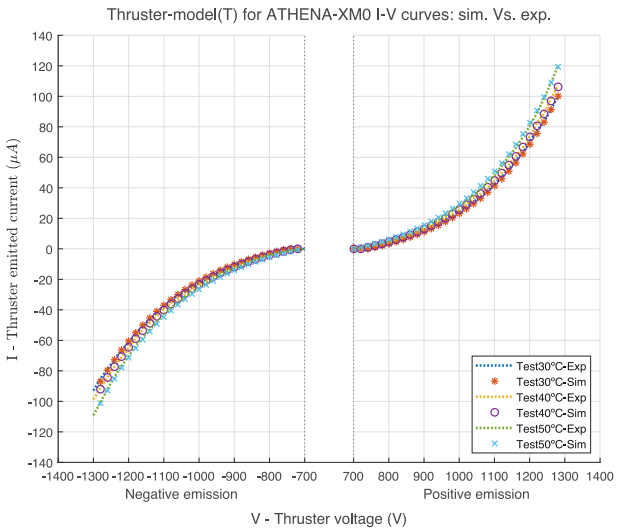

Fig. 11. Athena-XM0 *I–V* curves (emission area): real versus simulated (T).

In this case, the error is slightly higher compared with the approximation of a single curve at a fixed temperature. This effect is coherent since it is a 3-D object and has more complexity and variation than a 1-D curve. The surface approximation benefits from a larger set of data points to capture all its variations and complexities. However, as observed in Fig. 12, the model absolute error is always below 2.75 μA and below 8% relative error in the operating range of 1000 to 1400 V and -1000 to -1400 V.

Therefore, based on the results, it has also been verified that the temperature-dependent model presented in this section represents accurately the real current–voltage behavior of an electrospray thruster with temperature dependency. Consequently, this model allows for predicting the behavior within the approximated surface. The extracted parameters from the experimental data can be easily stored in a lookup table and be selected depending on the desired simulation conditions.

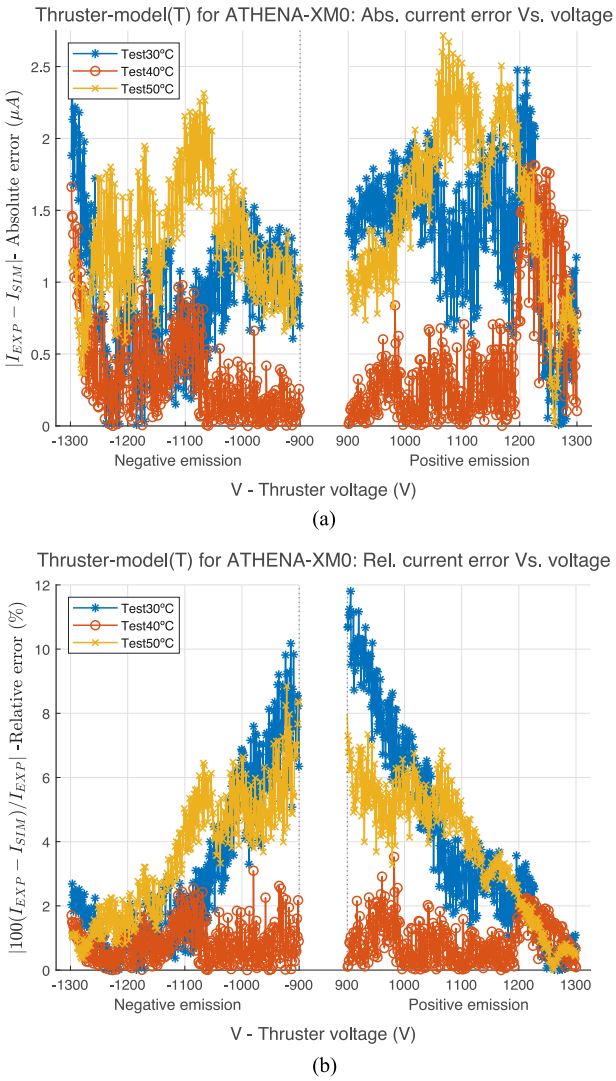

Fig. 12. Computed current error curves for Athena-XM0 experimental curves with the temperature dependent model. (a) Absolute error. (b) Relative error.

TABLE VII
TEST40°C—EXTRACTED COMPONENT VALUES FOR THE RESISTOR ABOVE START-UP VOLTAGE MODEL OF [18], [19], [20], AND[21]

Test40°C – Model C [18] [19] [20] [21]			
Component	**Equation (6) param.**	**Value**	**Units**
$D_{Z,P}$	V_0	952	V
R_P	R	3240	kΩ
$D_{Z,N}$	V_0	945	V
R_N	R	3840	kΩ

TABLE VIII
TEST40°C—EXTRACTED COMPONENT VALUES FOR RESISTOR+DIODE MODEL OF [23]

Test40°C – Model D [23]			
Component	**Equation (7) param.**	**Value**	**Units**
D_P	n	4752	-
	I_S	5931	μA
R_P	R	954	kΩ
D_N	n	4474	-
	I_S	3926	μA
R_N	R	1800	kΩ

TABLE IX
TEST40°C—EXTRACTED COMPONENT VALUES FOR THE EXPONENTIAL FUNCTION MODEL OF [15]

Test40°C – Model E [15]		
Component	**Equation (4) param.**	**Value**
Behavioral current source based on (4): $I = Xe^{YV}$	X_P	$144 \cdot 10^{-9}$
	Y_P	$52 \cdot 10^{-4}$
	X_N	$-110 \cdot 10^{-9}$
	Y_N	$53 \cdot 10^{-4}$

TABLE X
TEST40°C—EXTRACTED COMPONENT VALUES FOR THE PIECEWISE FUNCTION MODEL OF [17]

Test40°C – Model F [17]		
Component	**Equation (5) param.**	**Value**
Behavioral current source based on (5): $I(V) = \begin{cases} AV\left(e^{B\sqrt{V}}\right), & V \le V_0 \\ CV^2 + DV + E, & V > V_0 \end{cases}$	A_P	$1.68 \cdot 10^{-15}$
	B_P	$5.31 \cdot 10^{-1}$
	C_P	$5.26 \cdot 10^{-12}$
	D_P	$-9.10 \cdot 10^{-7}$
	E_P	$4.09 \cdot 10^{-4}$
	A_N	$-5.07 \cdot 10^{-9}$
	B_N	$-85 \cdot 10^{-4}$
	C_N	$-4.12 \cdot 10^{-10}$
	D_N	$-6.98 \cdot 10^{-7}$
	E_N	$-3.08 \cdot 10^{-4}$

A comparison of the models presented in this study with the models presented in the literature is included in Section VI.

VI. EXPERIMENTAL COMPARISON OF PRESENTED MODELS VERSUS PREVIOUS MODELS FROM LITERATURE

The objective of this section is to analyze and evaluate the behavior of the models presented in this article, the nontemperature-dependent and temperature-dependent models, in comparison to existing models in the literature, as described in Section III-A computing the Test40°C experimental data array. The values obtained by fitting this experimental curve to each model are given in Tables VII -X.

Table VI presents the comparison between the novel models presented in this article and models from the literature, including which components are needed to export the model to an electrical simulator, the model equation, literature reference, and error data. This table provides a clear and concise comparison of the models, where the models presented in this article offer better performance in terms of absolute and relative error and, therefore, are a significant contribution to the field.

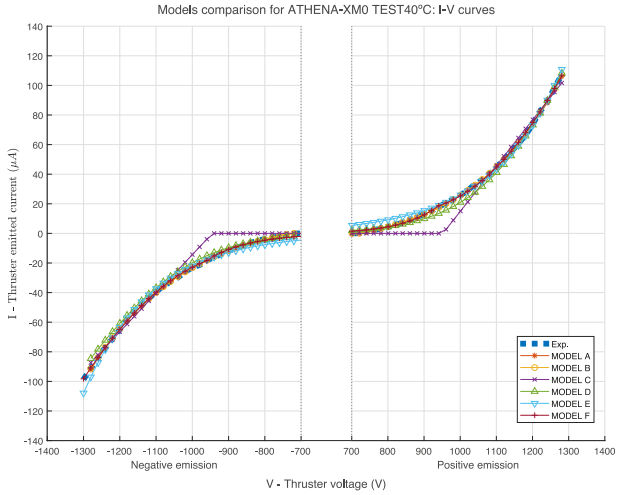

Fig. 13. Experimental *I–V* curve from Test40°C versus computed simulation models.

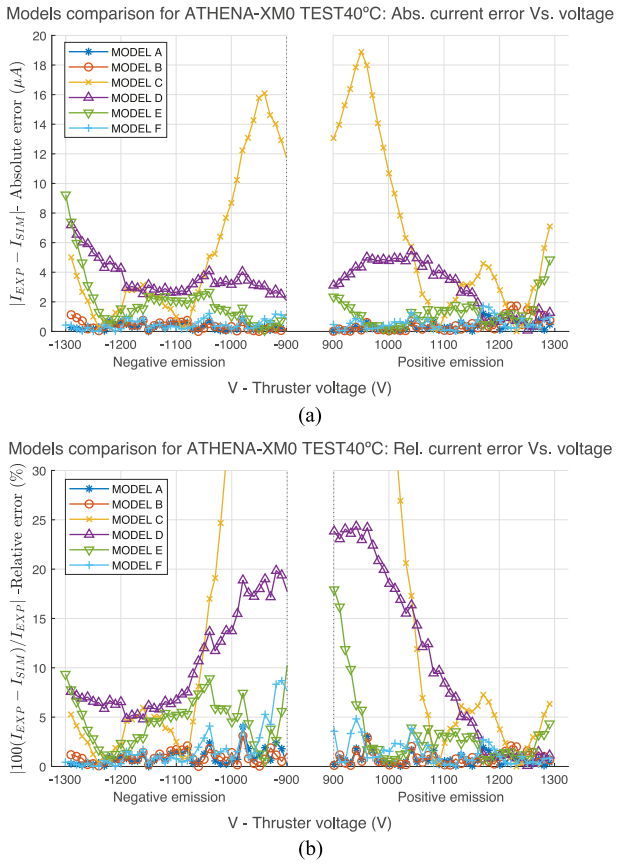

Fig. 14. Current error curves for Test40°C for the computed simulation models. (a) Absolute error. (b) Relative error.

Fig. 13 shows all the simulated *I–V* curves over the experimental data array while Fig. 14 includes the error plots for the models listed in Table VI.

As can be observed from the figures, Model C, which is based on an approximation through a resistor within the operation range, exhibits the poorest performance, as it fails to capture the nonlinearity inherent in electrospray thrusters. Model D, which

is based on a diode in series with a resistor, improves upon Model C by incorporating nonlinearity, but it still lags behind the models presented in this article. Model E, which uses a mathematical approximation within a behavioral current source, shows improved performance relative to Model D, but it is still limited by the approximations used. Model F, which is also based on a behavioral current source, offers improved performance but is not straightforward to extract the approximation parameters.

In contrast, the models presented in this article (Model A and Model B) offer the best performance, as demonstrated by their close agreement with the experimental data, as shown in Table VI. In addition, these results validates the temperature-dependent model presented in this article, which can predict the temperature behavior of the electrospray thruster based on a set of experimental input data.

VII. Conclusion

In this article, a comprehensive implementation of the electrical model for an electrospray thruster using basic electronic elements is presented. The model accurately captures the nonlinear and nonsymmetric behavior of the thruster across the minimum negative voltage to the maximum positive voltage applied to the thruster. The model parameters were extracted from the experimental data and validated through simulated curves, demonstrating its ability to accurately describe the behavior of the thruster. The model has been implemented using Simulink, but it is also capable of being used with any electrical simulator.

This implementation represents a significant contribution to the field, as it provides an improved means of conducting electrical simulations related to electrospray thrusters, improving load representation in the simulations of the power converters that supply the thrusters. In addition, the model could also be extrapolated in future works to mission analysis tools enabling quick exploration of a wide design space for the propulsion system [31] itself, its requirements, and the impact on the other subsystems and operations (e.g., increasing the fidelity in variable-ISP analysis [32]).

Furthermore, a novel temperature-dependent model is derived. A set of experimental data can be used to predict intermediate operation points. On the one hand, if a dataset of experimental curves is available, it would be advantageous to apply a temperature-dependent model to predict intermediate curves. On the other hand, if only a single curve is presented, the most appropriate model would be a nontemperature model.

Eventually, the models presented in this article have been compared with existing models in the literature using the same experimental input data and have been shown to provide a superior approximation since the absolute error compared with the best literature approximation is in the order of one microampere (which is an improvement of $\approx 26\%$ of percent error difference when compared) and is in the order of 1% of relative error (which is an improvement of 60% of percent error difference when compared).

The use of these models allows to store the extracted parameters from experimental data in a lookup table to be selected based on the desired simulation conditions. This approach is commonly used in a variety of fields to accurately model complex systems and make predictions that inform further experimentation.

Future work on this model will focus on incorporating additional factors that also affect the behavior of electrospray thrusters, such as arcs caused by extractor contamination, aging, spacecraft charging, and emitter degradation due to IL properties. This will allow for a more complete and accurate representation of the behavior of electrospray thrusters for lifetime simulations.

References

[1] T. Henning, K. Huhn, L. W. Isberner, and P. J. Klar, "Miniaturized electrospray thrusters," *IEEE Trans. Plasma Sci.*, vol. 46, no. 2, pp. 214–218, Feb. 2018, doi: 10.1109/TPS.2017.2755373.

[2] D. Krejci and P. Lozano, "Space propulsion technology for small spacecraft," *Proc. IEEE*, vol. 106, no. 3, pp. 362–378, Mar. 2018, doi: 10.1109/JPROC.2017.2778747.

[3] J. Mueller, R. Hofer, and J. Ziemer, "Survey of propulsion technologies applicable to cubesats," in *Proc. 57th JANNAF Propulsion Meeting*, 2015, pp. 32–40. [Online] Available: https://hdl.handle.net/2014/41627

[4] A. R. Tummala and A. Dutta, "An overview of cube-satellite propulsion technologies and trends," *Aerospace*, vol. 4, no. 4, 2017, Art. no. 58, doi: 10.3390/aerospace4040058.

[5] M. Turzynski and W. J. Kulesza, "A simplified behavioral MOSFET model based on parameters extraction for circuit simulations," *IEEE Trans. Power Electron.*, vol. 31, no. 4, pp. 3096–3105, Apr. 2016, doi: 10.1109/TPEL.2015.2445375.

[6] A. Edpuganti, V. Khadkikar, M. S. E. Moursi, H. Zeineldin, N. Al-Sayari, and K. Al Hosani, "A comprehensive review on CubeSat electrical power system architectures," *IEEE Trans. Power Electron.*, vol. 37, no. 3, pp. 3161–3177, Mar. 2022, doi: 10.1109/TPEL.2021.3110002.

[7] M. Yaqoob, A. Lashab, J. C. Vasquez, J. M. Guerrero, M. E. Orchard, and A. D. Bintoudi, "A comprehensive review on small satellite microgrids," *IEEE Trans. Power Electron.*, vol. 37, no. 10, pp. 12741–12762, Oct. 2022, doi: 10.1109/TPEL.2022.3175093.

[8] J. F. De La Mora and I. G. Loscertales, "The current emitted by highly conducting taylor cones," *J. Fluid Mechanics*, vol. 260, pp. 155–184, 1994.

[9] C. S. Coffman, "Electrically-assisted evaporation of charged fluids: Fundamental modeling and studies on ionic liquids," Ph.D. dissertation, Space Propulsion Lab., Massachusetts Inst. Technol., Cambridge, MA, USA, 2016.

[10] P. Lozano and M. Martinez-Sanchez, "Ionic liquid ion sources: Suppression of electrochemical reactions using voltage alternation," *J. Colloid Interface Sci.*, vol 280, pp. 149–54, 2004.

[11] B. Kang, K. -S. Low, J. J. Soon, and Q. -V. Tran, "Single-switch quasi-resonant DC–DC converter for a pulsed plasma thruster of satellites," *IEEE Trans. Power Electron.*, vol. 32, no. 6, pp. 4503–4513, Jun. 2017, doi: 10.1109/TPEL.2016.2600035.

[12] M. Fu, D. Zhang, and T. Li, "A novel coupling method of power supplies with high power density, efficiency, and fast dynamic response for spacecraft hollow cathode power supply applications," *IEEE Trans. Power Electron.*, vol. 32, no. 7, pp. 5377–5387, Jul. 2017, doi: 10.1109/TPEL.2016.2610442.

[13] P. D. Prewett and G. L. R. Mair, *Focused Ion Beams From Liquid Metal Ion Sources*. Somerset, U.K.: Res. Stud. Press, 1991.

[14] J. F. Mora, G. J. Van Berkel, C. G. Enke, R. B. Cole, M. Martinez-Sanchez, and J. B. Fenn., "Electrochemical processes in electrospray ionization mass spectrometry," *J. Mass Spectrometry*, Vol. 35, no. 8, pp. 939–952, Aug. 2000, doi: 10.1002/1096-9888(200008)35:8<939::AID-JMS36>3.0.CO;2-V.

[15] L. F. Velasquez-Garcia, A. I. Akinwande, and M. Martinez-Sanchez, "A planar array of micro-fabricated electrospray emitters for thruster applications," *J. Microelectromech. Syst.*, vol. 15, no. 5, pp. 1272–1280, Oct. 2006, doi: 10.1109/JMEMS.2006.879710.

[16] A. S. Sedra and K. C. Smith, "Microelectronic circuits," in *Oxford University Press*, NY, USA: New York: Holt Rinehart and Winston, 2004.

[17] F. Hicks, "Spacecraft charging and attitude control characterization of electrospray thrusters on a magnetically levitated testbed," Ph.D. dissertation, Space Propulsion Lab., Massachusetts Inst. Technol., Cambridge, MA, USA, 2017.

[18] N. Weiser, "Dual high-voltage power supply for use on board a CubeSat," *Ms.C. Dissertation, Elect. Eng. Dept*., California Polytechnic State Univ., San Luis Obispo, CA, USA, 2014.
[19] B. P. Baddipadiga, S. Strathman, M. Ferdowsi, and J. W. Kimball, "A high-voltage-gain DC-DC converter for powering a multimode monopropellant-electrospray propulsion system in satellites," in *Proc. IEEE Appl. Power Electron. Conf. Expo.*, 2018, pp. 1561–1565, doi: 10.1109/APEC.2018.8341224.
[20] J. Eisen, B. Cline, S. P. Berg, and J. Rovey, "Power processing unit and feed system development for a multimode spacecraft propulsion system," in *Proc. AIAA Propulsion Energy Forum*, 2021, doi: 10.2514/6.2021-3428.
[21] K. J. Prasad Veeramraju and J. W. Kimball, "An improved power processing unit for multi-mode monopropellant electrospray thrusters for satellite propulsion systems," in *Proc. IEEE Energy Convers. Congr. Expo.*, 2019, pp. 1302–1309, doi: 10.1109/ECCE.2019.8913026.
[22] B. Buso and P. Mattavelli, *Digital Control in Power Electronics*, 2nd ed. Williston, Vermont, USA: Morgan & Claypool Publishers, 2015.
[23] F. A. Hill, E. V. Heubel, P. P. de Leon, and L. F. Velásquez-García, "High-throughput ionic liquid ion sources using arrays of microfabricated electrospray emitters with integrated extractor grid and carbon nanotube flow control structures," in *J. Microelectromech. Syst.*, vol. 23, no. 5, pp. 1237–1248, Oct. 2014, doi: 10.1109/JMEMS.2014.2320509.
[24] M. Jordan and J. A. O'Connor, "Resonant fluorescent lamp converter provides efficient and compact solution," in *Proc. Eighth Annu. Appl. Power Electron. Conf. Expo.*, 1993, pp. 424–431, doi: 10.1109/APEC.1993.290695.
[25] D. Villegas-Prados, "Impact of the propellant temperature on the performance of externally wetted electrospray thrusters," in *Proc. Int. Electric Propulsion Conf.*, 2022, pp. 9–10.
[26] A. P. Froba, H. Kremer, and A. Leipertz, "Density, refractive index, interfacial tension, and viscosity of ionic liquids [EMIM][EtSO4],[EMIM][NTf2],[EMIM][N (CN) 2], and [OMA][NTf2] in dependence on temperature at atmospheric pressure," *J. Phys. Chem. B.*, vol. 112, no. 39, 2008, pp. 12420–12430, doi: 10.1021/jp804319a.
[27] T. Makino, M. Kanakubo, Y. Masuda, T. Umecky, and A. Suzuki, "CO2 absorption properties, densities, viscosities, and electrical conductivities of ethylimidazolium and 1-ethyl-3-methylimidazolium ionic liquids," *Fluid Phase Equilibria*, vol. 362, pp. 300–306, 2014, doi: 10.1016/j.fluid.2013.10.031.
[28] R. Khalil, N. Chaabene, M. Azar, I. B. Malham, and M. Turmine, "Effect of the chain lengthening on transport properties of imidazolium-based ionic liquids," *Fluid Phase Equilibria*, vol. 503, 2020, Art. no. 112316, doi: 10.1016/j.fluid.2019.112316.
[29] N. Siegel, "Silicon wafer integration of ion electrospray thrusters," Ms.C. dissertation, Space Propulsion Lab., Massachusetts Inst. Technol., Cambridge, MA, USA, 2020.
[30] C. Sarkar, "Thermal thinning of magnetorheological fluid and its effect on MR brake performance," *Int. J. Curr. Eng. Technol.*, vol. 5, no. 2, pp. 1100–1103, 2015.
[31] G. Di Pasquale, M. Sanjurjo Rivo, and D. Perez-Grande, "Space mobility optimization and concurrent engineering for modular micro-propulsion systems with 360 by IENAI SPACE," in *Proc. 73rd Int. Astronautical Congr.*, 2022, pp. 1–3.
[32] G. Di Pasquale, M. Sanjurjo Rivo, and D. Perez-Grande, "A novel variable-specific impulse optimization methodology for modulable electric propulsion systems," in *Proc. AIAA SciTech Forum*, 2023, doi: 10.2514/6.2023-2646.

Francisco José Blázquez-Plaza received the B.Sc. degree in telecommunications engineering from the University of Granada, Granada, Spain, in 2019, and the M.Sc. degree in industrial electronics from the Polytechnic University of Madrid, Madrid, Spain, in 2020. He is currently working toward the joint Ph.D. degree in power topologies for electrospray propulsion with the Universidad Carlos III de Madrid and IENAI SPACE, Madrid, Spain.

He is the Lead Electronics Engineer with IENAI SPACE. His current research interests include power electronics, energy efficiency, semiconductors, control algorithms, and electrospray propulsion.

Andrés Barrado (Senior Member, IEEE) received the M.Sc. degree in electrical engineering from the Polytechnic University of Madrid, Madrid, Spain, in 1994, and the Ph.D. degree in electrical engineering from Carlos III University of Madrid, Madrid, in 2000.

Since 2004, he has been a Full Professor with the Carlos III University of Madrid and the Head of the Power Electronics Systems Group (GSEP). He has been actively involved in moe than 85 R&D projects for companies in Europe and the U.S, and more than 25 projects with public funding, in the field of power electronics. He is Co-Founder of the spin-off company Power Smart Control S.L. oriented to applications and CAD for power electronics. He has authored or coauthored more than 200 scientific papers in international journals and conference proceedings and holds 12 patents. His research interests include switching-mode power supply, solar and fuel cell conditioning, behavioral modeling of converters and systems, fuel cell electric vehicle, power distribution systems for aircraft, and electromagnetic compatibility.

Mick Wijnen received the B.Sc. degree in applied physics from the Eindhoven University of Technology, Eindhoven, The Netherlands, in 2014, the M.Sc. degree in aerospace engineering from the Delft University of Technology, Delft, The Netherlands, in 2017, and the Ph.D. degree in fluid mechanics, with a focus on diagnostic techniques for the development of electric space propulsion, from the Universidad Carlos III de Madrid, Getafe, Spain, in 2023.

He is the CTO of IENAI SPACE, Madrid, Spain, where he is an in charge of the development of electrospray propulsion for nanosatellites.

David Villegas-Prados received the B.Sc. degree in aerospace engineering from the University Carlos III de Madrid, Madrid, Spain, in 2018, and the M.Sc. degree in space engineering (SpaceMaster) from Luleå University of Technology, Luleå, Sweden, and Université Toulouse III Paul Sabatier, Toulouse, France, in 2020. He is currently working toward the joint Ph.D. degree in electrospray propulsion and testing diagnostics with the Universidad Carlos III de Madrid IENAI SPACE, Madrid, Spain.

His current research interests include electric propulsion technologies, space exploration, indirect diagnostics, and electrospray propulsion.